ISSW23

Paper 1047

Hypervelocity Capability of the HYPULSE Shock-Expansion Tunnel for Scramjet Testing

R. O. Foelsche*, R. C. Rogers[†], C.-Y. Tsai*,
R. J. Bakos*, and A. T. Shih[†]

* GASL, Inc. Ronkonkoma, NY
[†] NASA Langley Research Center, Hampton, VA

International Symposium on Shock Waves, 23rd

July 22 – 27, 2001
Ft. Worth, Texas USA

Hypervelocity Capability of the HYPULSE Shock-Expansion Tunnel for Scramjet Testing

Robert O. Foelsche[1], R. Clayton Rogers[2], Ching-Yi Tsai[1], Robert J. Bakos[1], and Ann T. Shih[2]

[1] GASL, Inc., 77 Raynor Avenue, Ronkonkoma, NY 11779
[2] NASA Langley Research Center, Hampton, VA 23681

Abstract. New hypervelocity capabilities for scramjet testing have recently been demonstrated in the HYPULSE Shock-Expansion Tunnel (SET). With NASA's continuing interests in scramjet testing at hypervelocity conditions (Mach 12 and above), a SET nozzle was designed and added to the HYPULSE facility. Results of tests conducted to establish SET operational conditions and facility nozzle calibration are presented and discussed for a Mach 15 (M15) flight enthalpy. The measurements and detailed computational fluid dynamics calculations (CFD) show the nozzle delivers a test gas with sufficiently wide core size to be suitable for free-jet testing of scramjet engine models of similar scale as those tested in conventional low Mach number blow-down test facilities.

1 Introduction

In 1996 NASA's HYPULSE facility [1][2], located at and operated by GASL, Inc., was converted from a Shock-Expansion Tube to a Reflected-Shock-Tunnel (RST) to permit free-jet testing of subscale scramjet engine flowpaths at flight Mach numbers of 7 and 10. The conversion changes included the addition of a 2.13-m (84-in.) diameter test cabin and a 0.66-m (26-in.) exit-diameter contoured supersonic nozzle, with an area ratio of 175 (AR-175). Upgrades and changes to existing facility hardware were made to install a detonation driver to obtain reflected-shock operation at higher-pressure. The design and configuration changes to obtain RST mode were made so that operational changes from reflected-shock to shock-expansion mode could be done in about a day.

The detonation driver made possible tube exit pressures high enough to operate HYPULSE as a Shock-Expansion Tunnel (SET) by adding a diverging nozzle to the end of the acceleration tube. The new SET nozzle, with an area ratio of 16 (AR-16), was designed at GASL for a prescribed M21 flight condition, and had a hyperbolic contour that approached a 10° half-angle cone at the exit. In SET configuration the facility can deliver test conditions suitable for scramjet tests up to Mach 16 (M16) flight speed duplication [3] and atmospheric re-entry simulations up to Mach 25. Exit pitot measurements and detailed CFD show the nozzle delivers a test gas flow with a sufficiently wide core size at the M15 condition, to be suitable for free-jet testing of scramjet engine models. Details of the SET nozzle design and M21 condition are presented in a separate paper presented at this symposium [4].

The HYPULSE facility is now a dual-mode facility that can be configured in either RST or SET mode depending on the desired simulation. The current paper describes the RST to SET conversion, the facility nozzle calibration tests, and determination of test conditions for M15 operation.

2   Experiment and Operation

For the SET mode, HYPULSE is operated by a short (0.61-m (2-ft.) long) cold helium driver at pressures up to 83 MPa (12,000 psi) in conjunction with a detonation driver, that is the upstream portion (7.7-m (25.3-ft.) long) of the shock tube section. All shock tube sections are 15.2-cm (6 in.) diameter. The detonation driver contains a stoichiometric hydrogen-oxygen mixture diluted with a noble gas, and is separated from the helium driver by a double steel-diaphragm section. The detonation tube is followed by the 5.1-m (16.8-ft) long intermediate tube that contains the test gas. The downstream 12.5-m (41 ft) long section of the tube is used as the acceleration tube. A Cirlex diaphragm (typically 1 mm thick) separates the detonation and intermediate tubes and the intermediate and acceleration tubes are separated by a thin Mylar diaphragm (typically 0.025 mm thick). The acceleration tube is connected to the SET AR-16 contoured nozzle. As indicated in Fig. 1, the nozzle is bolted to the shock tube end and rides on a rail inside the test section. The shock tube-nozzle pieces are coupled to the test section with a sealed slip-joint that allowed the test section to recoil as the shock tube vents post-test.

Changing the HYPULSE configuration between RST and SET mode requires removal of the RST throat and contoured sections of the nozzle and the RST mating joint to the test section, and replacement of these items with the SET open-ended tube extension, the slip joint, and AR-16 contoured nozzle. In addition, a relatively easy shortening of the He driver section is required.

The shock wave generated by the sudden rupture of the double diaphragm passes into the detonable mixture (typically 30 H_2 + 15 O_2 + 55 He) and forms a stronger shock front to heat and compress the low-pressure gas in the intermediate tube that will become the test gas. The test gas processed by passage of the incident shock is accelerated by an unsteady expansion fan to a steady flow at the tube exit, achieving very high enthalpy through the addition of kinetic energy, without being stagnated. The acceleration tube is evacuated to the same level as the nozzle and test hardware contained in the test section. The processed test gas is expanded by the AR-16 nozzle from the initial acceleration tube diameter to the nozzle exit state for the desired test condition. Resulting test times of HYPULSE in SET mode are short, on the order of a few hundred microseconds of steady flow, which allows for the use of less complicated and less expensive un-cooled engine and model hardware fabricated from stainless steel and aluminum. Additional details and descriptions of HYPULSE operation are in the literature [1] [2] [3].

Test conditions were determined from initial pressure and temperature of the shock tube fill gases and measured shock speeds. The shock speeds were based on

shock arrival times recorded by fast-response, flush wall-mounted, piezoelectric quartz-crystal pressure sensors (PCB Piezotronics, Inc., model 113A24 typical) distributed along the shock tube. Four sensors were used at fixed locations in the intermediate tube and six sensors in the acceleration tube. Two static pressure measurements were taken 5 cm upstream of the tube exit (nozzle entrance) with high sensitivity gages (model 112A22 typical). This information was used along with the gas compositions in each tube to calculate post-shock gas properties. A shock speed calculated from the measured arrival times at two successive locations was assumed to apply at the mid-point of the two locations. The primary shock speed (in the intermediate tube) exhibited a linear-decrease between the measurement points. These measured shock speeds were curve-fit and extrapolated to the interface with the acceleration tube. Similarly, the last three shock speeds calculated for the acceleration tube showed a linear trend over the last 2.3 m of the tube and were extrapolated to the nozzle entrance. The shock speeds had an uncertainty of about one percent.

Several calibration tests at various shock tube initial pressure ratios were run to define the tube exit conditions for the desired M15 operation. The conditioning tests included pitot pressure surveys obtained at the tube exit (no nozzle) to aid in calculating test gas conditions at the tube exit and to derive inflow conditions for a CFD calculation of the nozzle exit flow. From these tests an empirical correlation was also obtained for the tube exit static temperature.

The post-primary shock condition state (2) was calculated from the intermediate tube initial fill condition state (1) (P_1, T_1, gas composition) and measured shock speed ($U_{s,1}$) using a 1-D equilibrium code. It was assumed that chemical equilibrium was achieved across the normal shock wave front. After passage of the incident shock, the test gas at state (2) was accelerated by an unsteady expansion to a steady condition at the tube exit. The tube exit Mach number M_5 was calculated from the ratio of measured tube end centerline pitot pressure ($P_{t2,5}$) and measured static pressure (P_5) by the approximate pitot relation $M_5 = 0.9(P_{t2,5}/P_5)^{0.5}$. The static temperature T_5 was calculated from M_5, U_5, and γ_2 via $T_5 = (U_5/M_5)^2/(R_{air}\gamma_2)$, assuming the flow velocity (U_5) has reached the measured shock velocity ($U_5 = U_{s,2}$) on centerline, and where R_{air} is the gas constant for air and γ_2 is the ratio of specific heats behind the primary shock. The post-secondary shock condition at the end of the tube was calculated from the measured P_5 and $U_{s,2}$ and calculated T_5 using the 1-D equilibrium code. State (5) flow properties were assumed to hold only at the centerline of the tube, except for the assumed uniform static pressure P_5.

Calibration of the shock tube was completed by computing an ideal value of T_5 by isentropically expanding the flow from the pressure at state (2) to the measured P_5 using the relation $T_{5,id} = T_2(P_5/P_2)^{((\gamma_2-1)/\gamma_2)}$. This information provided a means to obtain the tube-end temperature through the correlation of $T_5/T_{5,id}$ for tests such as nozzle surveys and engine tests without tube-end pitot pressure data.

For nozzle calibration and model tests, the expansion tube exit state was determined from data values of exit pressure P_5, the incident and secondary shock

speeds, and the temperature T_5 from the shock tube calibration. The state (2) condition was calculated as already described. The ideal centerline temperature at state (5) was calculated and the actual T_5 obtained from the expansion tube correlation. Once T_5 was known, the post-secondary shock condition was calculated using P_5 and $U_{s,2}$ with the 1-D equilibrium calculation.

To date, test points have been established for nominal flight M15 and M21 conditions in SET mode as described. To produce the M15 flight enthalpy, the tube operational pressures were: driver fill pressure P_4 = 20.68 MPa (3000 psi); detonation tube fill pressure P_{100} = 689 kPa (100 psia); intermediate tube fill pressure P_1 = 91.9 kPa (13.3 psia); and acceleration tube fill pressure P_{10} = 91.9 Pa (0.013 psia). The resulting nominal facility tube exit (nozzle inlet) conditions are H_{pl} = 11.5 MJ/kg (4960 BTU/lb), P_{pl} = 1600 MPa (232 kpsi) and T_{pl} = 7730 K (13920 R), where "pl" is the plenum condition for an effective stagnation state reached by an isentropic process in chemical equilibrium.

3   Facility Flow Measurements

Two tests at the finalized facility operating condition were conducted to obtain a single tube exit pitot pressure profile. Measurements were made with a five-probe rake with pressure sensors calibrated in-situ to 3.45 MPa (500 psia). The inter-probe spacing was 2.5 cm (1 in.) and the two tests differed by off-setting the rake 1.27 cm radially on the tube centerline to obtain 10 total data points over the 15.4-cm dia. tube. The data were fitted with a sixth-order polynomial that gave a nominal centerline pitot pressure of approximately 3.1 MPa (447 psia), and stayed within 90% of the centerline value over a 2.5-cm dia. inner core region. The centerline value, when normalized by the tube exit pressure ($P_{t2,5}/P_5$ = 73.9), was taken as a benchmark for subsequent tests.

Four facility nozzle exit pitot pressure surveys were conducted with a 27-probe rake instrumented with model 112A22 piezocrystal pressure sensors that were calibrated in-situ to 138 kPa (20 psia). The rake had an inter-probe spacing of 2.5 cm and each probe had a 0.24 cm (0.093 in.) dia. hole at the tip. A B-screen was installed to protect the gage diaphragm. The probe tip had a flat face 0.76-cm (0.30 in.) dia. followed by a 15° half-angle cone out to 1.27-cm (0.50 in.) dia. Measurements were taken at axial locations (x) of 2.5, 20, and 38 cm (1, 8, and 15 in.) from the nozzle exit plane. The data and computed profiles are shown in Fig. 2 and Fig. 3 for each axial location. The pitot pressures are normalized by the static pressure P_5 measured at the shock tube/nozzle interface, to remove test-to-test variations.

A 1.9-cm (0.75 in.) diameter reference hemisphere for measuring stagnation heating was installed on the pitot rake for the nozzle surveys at x=20 and 38 cm. The hemisphere was instrumented with thin-film, resistance thermometers painted onto the solid Macor ceramic hemisphere at 0 (stagnation point), ±15°, ±30°, and ±60°. The thin film gage is a platinum strip, 0.89 mm (0.035 in.) long by 0.05 mm (0.002 in.) wide; the gages are manufactured and calibrated at GASL. The hemisphere was installed on an outrigger attached to the pitot rake,

9.2 cm (3.6 in.) off nozzle centerline. The derived heating rates q are plotted in Fig. 4. Curve fits of the form $q(\phi) = a_1 \cos^{2/3}(\phi) + a_2$, suggested by measurements from various other sources [5], are superposed on the data and show quite good matching, once the fit for the data at x=20 cm had been shifted by 15°.

4   Analysis

The tube exit pitot pressure profile indicated that the tube exit velocity was highly non-uniform due to viscous effects. Two-dimensional profiles of flow properties were obtained at tube-end by assuming the velocity profile in the axisymmetric flow was close to fully developed pipe flow and could be approximated by a one-fifth power law. The centerline velocity was determined from the measured shock speed with Mirels laminar boundary layer analysis correction applied. The static pressure was assumed constant across the flow (at the measured P_5 value) and the static temperature profile derived from fluid dynamics [6]. These profiles provided input conditions to a CFD code to compute the nozzle exit conditions, particularly the pitot pressure. The comparison between the computed nozzle exit pitot profiles with data is shown in Fig. 2 and Fig. 3. The CFD results and data agree quite well at all three axial stations, indicating that the tube-end profile assumptions are valid.

The nozzle exit core size, which was taken as the region where the pitot pressure is within 90% of the mean, was about 25-cm diameter. The core diameter based on data remained essentially 25-cm out to x=38 cm, but the computed results showed a gradual growth from 25 to 30 cm. The pitot data in the figures showed that, in the core, $P_{t,2}/P_5$ decreased with axial distance slightly more rapidly than predicted by the CFD. The nozzle was designed with an exit profile approaching a 10° conical expansion and thus the flow continues to expand after exiting the nozzle, a trend confirmed by CFD predictions. At x=2.5 cm, measurements and computed results show fine agreement outside the 25 cm core but poorer agreement within the core out to about radius $r = \pm 12$ cm. It was observed that the probe tips in the core flow deteriorated rather quickly from test-to-test as a suspected result of impacts from the plastic diaphragm particulates. The flat faces of the probe tip became pitted and dented, that resulted in a rough-edged probe hole, which may have contributed to measurement deterioration in successive tests. The survey at x=2.5 cm was the last nozzle calibration test performed.

The deterioration in the quality of the core pitot measurements as a result of damaged probe tips can be confirmed by the two independent surveys at x=20 cm. These data profiles show good repeatability between tests where one case (solid symbols) shows the best overall agreement with the computed profile and the other case (open symbols, measured earlier in a different test program) showed more scatter within the core. At x=38 cm the measured mean core pressure is 12% below the prediction and shows a similar trend out to 50-cm diameter but excellent agreement in the wings of the profile at both positive

and negative radial locations. The causes for this disparity remain unclear, but it points to the age-old problem of secondary diaphragms in expansion tubes.

The AR-16 nozzle exit had a calculated core flow with $M_e = 13.5$, $P_e = 0.656$ kPa (0.095 psia), $T_e = 315$ K (567 R), and $V_e = 4800$ m/s (14975 ft/sec). These nozzle exit flow conditions were calculated for the M15 condition using detailed CFD as described in Ref. [6].

The M15 flight enthalpy condition with HYPULSE in SET mode and the AR-16 nozzle has been used for preliminary tests of a scramjet engine model. The 48 cm (19-in.) wide flat forebody of the scramjet model had a "sharp" leading edge (nose radius ≈ 0.25 mm, 0.010 in.) and boundary layer trips to provide for boundary layer growth and 2-D flow capture. Static pressure measurements on the scramjet forebody are plotted in Fig. 5 for three typical tests and show good repeatability. A trend line drawn through the measurements indicates a decreasing pressure with axial distance that follows a quadratic form.

Schlieren and luminosity images of the forebody flow are shown in Fig. 6 for a forebody incidence angle of 8.0° to the tunnel flow. The shock from the forebody leading edge and the boundary layer trips and their interaction can be seen in the figure. The speckles in the image are on the windows and are not particulates in the flow. The luminosity image shows the high temperature boundary flow and stagnation region on a reference pitot probe mounted on a wedge beneath the leading edge.

5   Conclusions

The HYPULSE facility testing capability has been expanded to include Shock-Expansion Tunnel operation by the addition of an AR-16 facility nozzle used in conjunction with a detonation driven shock tube. To date Mach 15 and Mach 21 flight enthalpy conditions have been calibrated. The nozzle delivers a 25-cm diameter test gas core at M15 conditions that is suitable for free-jet testing of scramjet engine models. Calibration of the M15 condition and resulting nozzle exit pitot pressure surveys are discussed and were found to compare well to predictions from detailed computations. Preliminary scramjet engine testing has begun in support of NASA Langley scramjet research efforts and forebody static pressure measurements show clean, repeatable results. In conjunction with a Reflected-Shock Tunnel operational capability, the calibrated operational test points of HYPULSE Tunnel now includes Mach 7, 10, 15, and 21 flight enthalpy conditions.

References

1. Bakos, R.J., Calleja, J.F., Erdos, J.I., Sussman, M.A., and Wilson, G.J., "An Experimental and Computational Study Leading to New Test Capabilities for the HYPULSE Facility with a Detonation Driver," AIAA Paper 96-2193, Presented at

the 19th AIAA Advanced Measurement and Ground Testing Technology Conference, New Orleans, LA, USA, June 1996.

2. Bakos, R.J., Calleja, J.F., Erdos, J.I., Auslender, A.H., Sussman, M.A. and Wilson, G.J., "Design, Calibration, and Analysis of a Tunnel Mode of Operation for the HYPULSE Facility," AIAA Paper 96-2194, Presented at the 19th AIAA Advanced Measurement and Ground Testing Technology Conference, New Orleans, LA, USA, June 1996.

3. Erdos, J.I., Bakos, R.J., Castrogiovanni, A., and Rogers, R.C., "Dual Mode Shock Expansion/Reflected-Shock Tunnel," AIAA Paper 97-0560, Presented at the 35th Aerospace Sciences Meeting and Exhibit, Reno, NV, USA, January 1997.

4. Chue, R.S.M., Bakos, R.J., and Tsai, C.-Y., "The Design of an Expansion Tunnel Nozzle in HYPULSE," Paper 1046, Presented at the 23rd International Symposium on Shock Waves, Fort Worth, TX, USA, June 2001.

5. Anderson, J. D., "Hypersonic and High Temperature Gas Dynamics", McGraw-Hill, 1989, pp. 257-262.

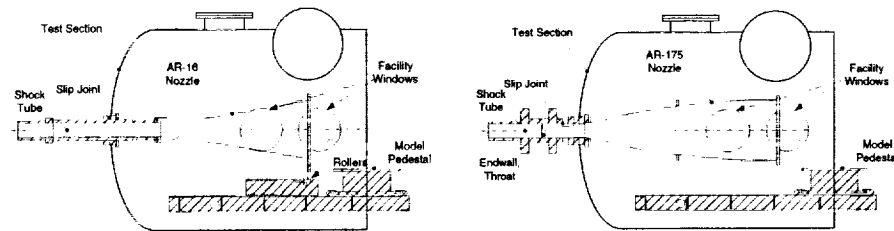6. Chue, R.S.M., GASL R&AD TN-134, May 2001.

Fig. 1. Schematic of SET (left) and RST (right) mode configuration in HYPULSE.
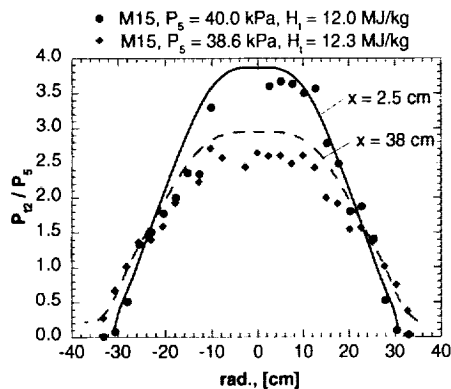

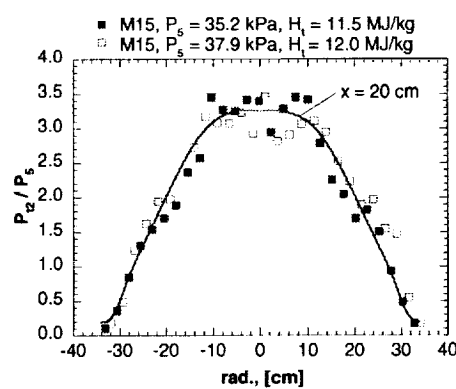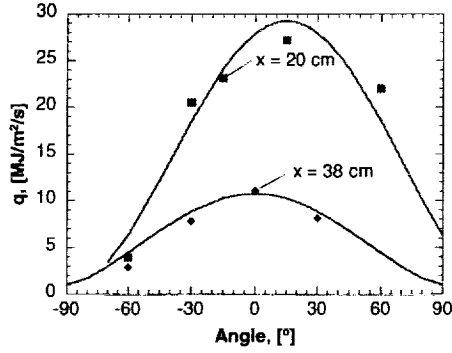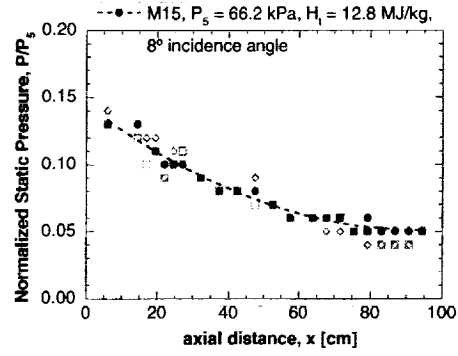**Fig. 2.** Measured pitot pressures and computed results at 2.5 and 38 cm from nozzle exit.

Fig. 3. Measured and computed pitot pressures 20 cm from the nozzle exit showing good repeatability.

Fig. 4. Measured heating on a hemisphere curve-fitted with typical $\cos^{2/3}(\phi)$ function.

Fig. 5. Measured static pressures on typical scramjet forebody at M15 flight enthalpy condition, for three individual tests, displaying quadratic decrease with axial distance.
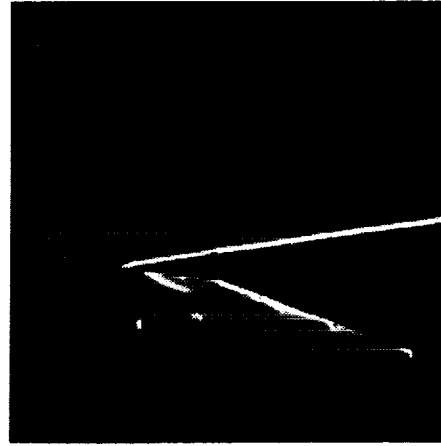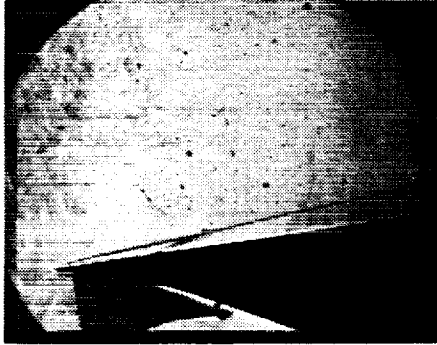
Fig. 6. Schlieren (left) and luminosity (right) images of engine forebody, with flowpath facing up.